Probabilistic Seismic Hazard Assessment for Pacific Island Countries

Y. Rong
FM Global, Norwood, MA, USA (formerly at AIR Worldwide, Boston, MA, USA)

J. Park & D. Duggan
AIR Worldwide, San Francisco, CA, USA

M. Mahdyiar
AIR Worldwide, Boston, MA, USA

P. Bazzurro
I.U.S.S., Pavia, Italy (formerly at AIR Worldwide, San Francisco, CA, USA)

SUMMARY:
A fully probabilistic earthquake hazard assessment study was carried out for fifteen Pacific Island Countries (PICs): Cook Islands, Fiji, Kiribati, Republic of Marshall Islands, Federated States of Micronesia, Nauru, Niue, Palau, Papua New Guinea, Samoa, Solomon Islands, Timor-Leste, Tonga, Tuvalu and Vanuatu. A regional seismicity model was built based on historical and instrumental earthquake catalogs, subduction zone segmentation and plate motion information, geodetic data, and available data on crustal faults. We used different ground motion prediction equations to account for different types of earthquakes. The effect of site conditions on ground motion was modeled based on shear wave velocities derived from microzonation studies and high-resolution topographic slope data. A comparison of our findings with those of earlier studies, such as GSHAP, shows similarities, and in some cases, significant differences. The seismic hazard maps developed here have a spatial resolution that is adequate for local seismic risk studies and building code applications.

Keywords: Probabilistic seismic hazard assessment (PSHA), Pacific Islands, seismicity model, ground motion

1. INTRODUCTION

Many of the PICs are located close to one of the most active subduction zones in the world and are prone to high seismic risk. Since the year 2000, fifteen earthquakes of moment magnitude (M_w) greater than or equal to 7.5 have occurred in the region, with four having M_w>8.0. The complicated tectonics and the high seismicity of the region are due mainly to the interaction of four major plates (Figure 1), the Pacific, Philippine Sea, Sunda, and Australia plates. The Philippine Sea plate subducts to the west under the Sunda plate at a rate of about 100 mm/year, and the Australia plate subducts to the north beneath the Sunda plate at a rate of about 70-80 mm/year. The convergence between the Australia and Pacific plates results in a shortening at the subduction plate boundaries along Papua New Guinea, the Solomon Islands, Vanuatu, Fiji and Tonga. The convergence rate is about 60-70 mm/year at the Tonga trench, and about 100 mm/year at other trenches.

Until this study, a consistent and up-to-date view of the seismic hazard for this region was not available in the open literature. The Global Seismic Hazard Assessment Program (GSHAP) conducted a uniform but coarse seismic hazard study for the entire region (McCue, 1999). In the present study, however, we include spatial resolution sufficient for local level applications, more recent ground motion prediction equations (GMPEs), and site effects. The seismic hazard of some countries such as Fiji, Papua New Guinea (PNG), and Vanuatu has been studied in more detail (e.g., Jones, 1998; Suckale and Grünthal, 2009), but the methodologies used were not the same for all regions and the resulting seismic hazard was not expressed in a uniform way across studies. Detailed seismic hazard studies for countries such as Tonga, Tuvalu, Samoa and the Solomon Islands are even rarer or non-existent in the open literature. As part of the Pacific Catastrophe Risk Assessment and Financing Initiative project funded by the World Bank and supported by other agencies, including the Asian Development Bank and the Applied Geoscience and Technology Division (SOPAC) of the Secretariat

of the Pacific Community, we developed country-specific seismic risk assessment models for fifteen PICs: Cook Islands, Fiji, Kiribati, the Republic of Marshall Islands, the Federated States of Micronesia, Nauru, Niue, Palau, Papua New Guinea, Samoa, Solomon Islands, Timor-Leste, Tonga, Tuvalu, and Vanuatu. The main objective of the hazard assessment component of this study was to create a uniform and detailed regional seismic hazard model that captures the spatial variation of the hazard and could be used to support realistic estimation of the earthquake ground shaking risk across the region. The study included modeling of earthquake-induced tsunami hazard, but that component is not covered here.

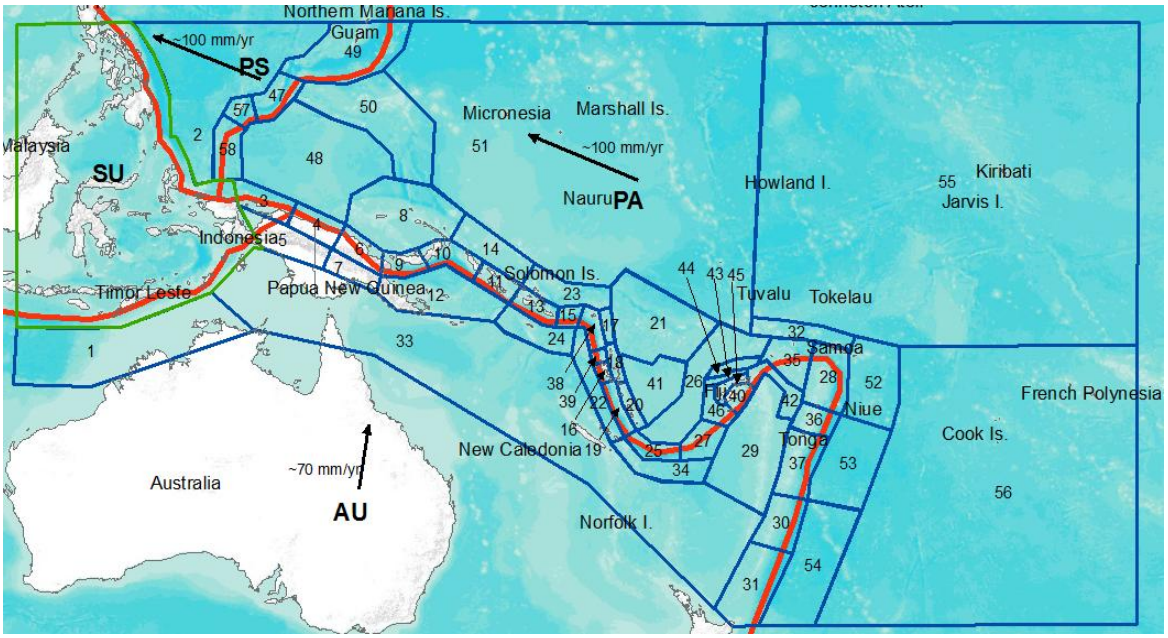

Figure 1. Regional tectonic setting and seismic source zones in the South Pacific region.Thick red lines indicate the major plate boundaries between the four major plates: Pacific (PA), Philippine Sea (PS), Sunda (SU), and Australia (AU) plates. Thick black arrows illustrate the movement of the PA, PS, and AU plates relative to the SU plate (Bird, 2003). The source zones are illustrated by blue polygons, and the numbers are the zone IDs. The area in the green polygon was covered by the AIR Southeast Asia earthquake model.

2. DATA

2.1 Historical earthquake catalogs

The availability of historical earthquake data for the Pacific Ocean region is limited compared to other parts of the world. To obtain a relatively complete, single catalog for the entire region, we selected, processed, and merged the following three historical earthquake catalogs:

1. PAGER-CAT by Allen et al. (2009) for the period 1900 – 2009,
2. Engdahl et al. (1998) relocated global earthquake catalog for the period 1964 – 2004, and
3. Earthquake database assembled by Geoscience Australia (http://www.ga.gov.au/earthquakes/searchQuake.do) for the period 1958 – 2009.

Before merging the catalogs, the magnitude values reported in the Engdahl et al. catalog (1998) were converted to moment magnitude, M_w, using the regression relationships established by Suckale and Grünthal (2009). The magnitudes other than M_w (the surface magnitude, M_S; the body wave magnitude, m_b; the local magnitude, M_L; the duration magnitude, M_D; and unknown magnitudes, M_{UK}) reported in PAGER-CAT were converted to M_w using the magnitude regression relationships derived in this study:

$$M_w = 0.8252M_s + 1.2188 \quad (2.1)$$

$$M_w = 0.7546m_b + 1.7809 \quad (2.2)$$

$$M_w = 1.3210M_L - 1.8631 \quad (2.3)$$
$$M_w = 0.8110M_{UK} + 1.2640 \quad (2.4)$$
$$M_w = 0.9644M_D + 0.4677 \quad (2.5)$$

Equations (2.1) through (2.4) were derived based on the PAGER-CAT data from the South Pacific region, while Equation (2.5) was derived from all the PAGER-CAT data. For events in PAGER-CAT with only the teleseismic body-wave magnitude, m_B, available, we used the relationship by Bormann and Saul (2008):

$$M_w = 1.33m_B - 2.36 \quad (2.6)$$

The events contained in the three historical earthquake catalogs were also augmented with an additional 42 large ($M_w \geq 7.0$) historical events that were identified from various publications. Some of them were recorded pre-1900.

Due to the remoteness of the region and poor coverage by seismographs, about 20% of the earthquakes in the merged historical earthquake catalog either lacked a hypocentral depth or had a default depth value (e.g., 33 km). The hypocentral depth for these events was probabilistically assigned based on empirically-based depth distributions derived from other historical events in this region. Finally, we declustered the merged catalog from foreshocks and aftershocks using the method of Reasenberg (1985). Figure 2 shows the epicenters of the historical earthquakes included in the final combined catalog (down to M_w 5.0; smaller events were not included in the plot). The completeness time in the catalog varies by region. Generally, the catalog is considered to be complete for events of M_w 5.3 or greater that have occurred since 1964. For Fiji and its vicinity, events of M_w 6.5 and greater are complete since 1910. For other regions, events of M_w 7.0 and greater are complete since 1900.

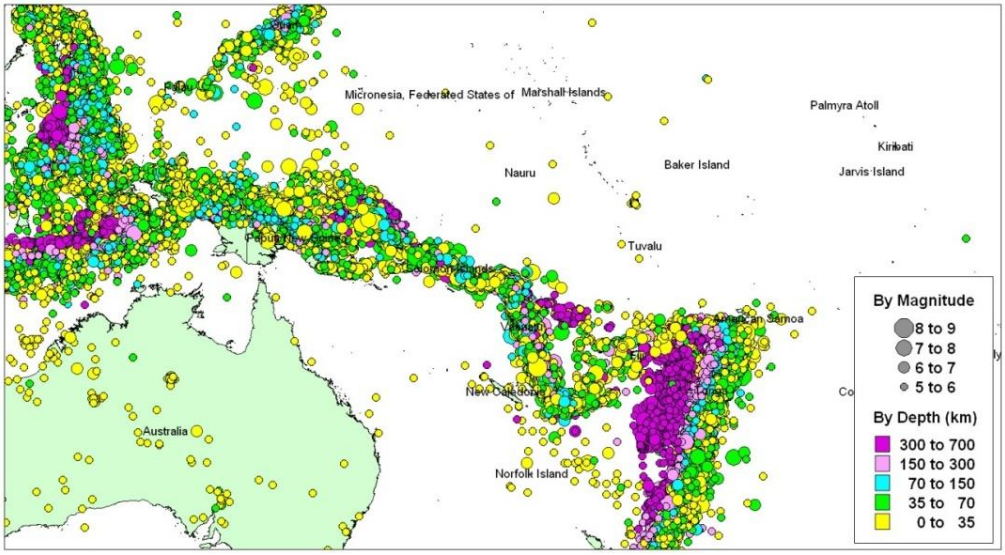

Figure 2. Epicenters of earthquakes in the Pacific Island Countries region contained in the merged historical catalog (down to M_w 5.0). Circles are color-coded by depth and sized by magnitude.

2.2 Subduction segments, crustal faults and geodetic GPS data

Among the fifteen PICs studied in this project, Palau, Papua New Guinea, Samoa, Solomon Islands, Vanuatu, Timor-Leste, and Tonga are located on or close to subduction zones. Segmentation models of subduction zones (e.g., Nishenko 1991), have been customarily considered as a guide to the location and extent of mega-thrust earthquakes. However, the validity of segmentation models in seismic hazard studies has been recently challenged by the most recent mega-thrust earthquakes: the 2004 Sumatra, Indonesia, the 2010 Maule, Chile, and the 2011 Tohoku, Japan earthquakes. Here we used segmentations as a model framework, but allowed some earthquakes to rupture multiple segments.

In addition to the subduction of plates, active crustal faults are potential sources of large earthquakes. For example, the 1953 Suva earthquake, the most damaging earthquake of Fiji in recent times, took place on a near-shore crustal fault. Potentially active faults have been identified in Viti Levu of the Fiji Islands (Rahiman, 2006), in PNG (Puntodewo et al., 1994; Tregoning et al., 1998), and in the Tonga-New Hebrides region (Pelletier et al., 1998). The crustal faults and subduction trenches are displayed in Figure 3.

We used a total of 254 GPS velocity vectors from various sources: Simons et al. (2007), Wallace et al. (2004), Calmant et al. (2003), Tregoning et al. (1998), Bevis et al. (1995), Puntodewo et al. (1994), Dawson et al. (2010, personal communications, IAG data), and Wallace et al. (2010, personal communications, GNS data). The spatial distribution of these GPS stations is uneven (Figure 3). Along the subduction zone, PNG and Vanuatu have the best coverage, whereas we could not locate any GPS measurements in the Solomon Islands. The GPS stations on the Sunda plate (Figure 1) are not included here since that region was already covered in the AIR Southeast Asia earthquake model (2004), which is not discussed here.

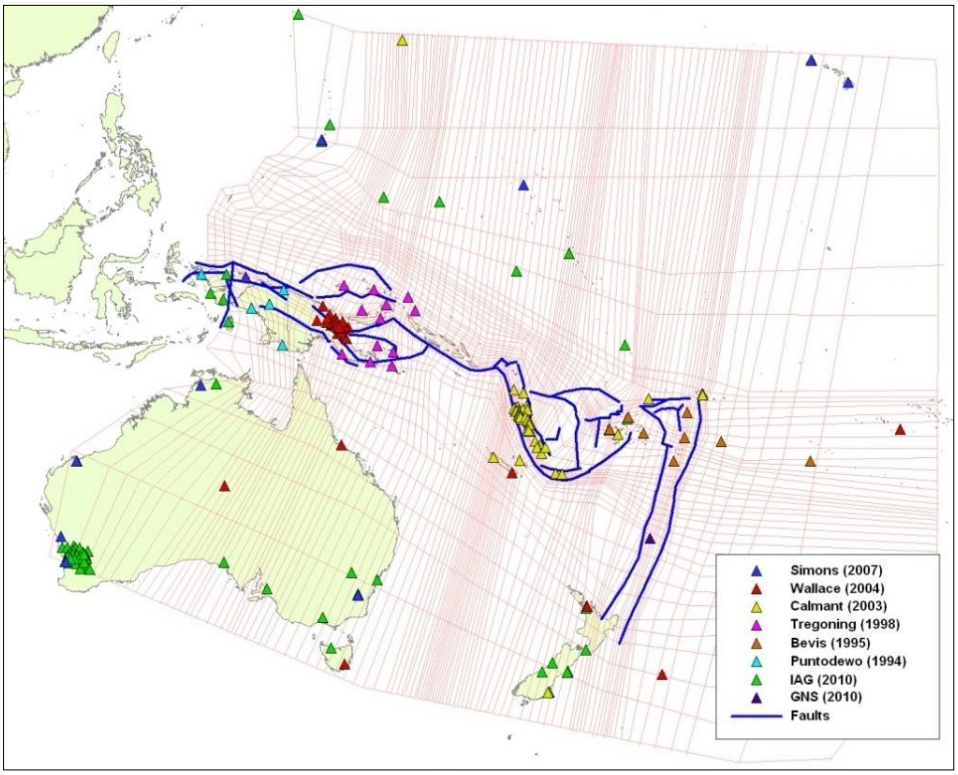

Figure 3. Location of GPS stations (triangles) used in this study. The pink lines illustrate curvilinear grids used in our regional kinematic model. Subduction trenches and geological faults are displayed in thick blue lines.

3. KINEMATIC MODELING BASED ON GPS AND ACTIVE FAULTS DATA

We used the 254 GPS velocity vectors and the active faults data shown in Figure 3 to invert the regional strain rate field using the well-established methodology by Haines and Holts (1993) and Haines et al. (1998). We also adopted the relative plate motion between the Australia and Pacific plates as a constraint in the inversion procedure to supplement the GPS and the active faults data. The relative plate motion was derived based on Global Strain Rate Map by Kreemer et al. (2003). The reference frames of the data include ITRF94, ITRF2000, ITRF2005, No-Net-Rotation (NNR), stable Pacific Plate, and stable Australia Plate. In the inversion, the original reference frame of each individual study was left undefined a priori, and then it was solved upon fitting geodetic velocities to one self-consistent velocity gradient tensor field.

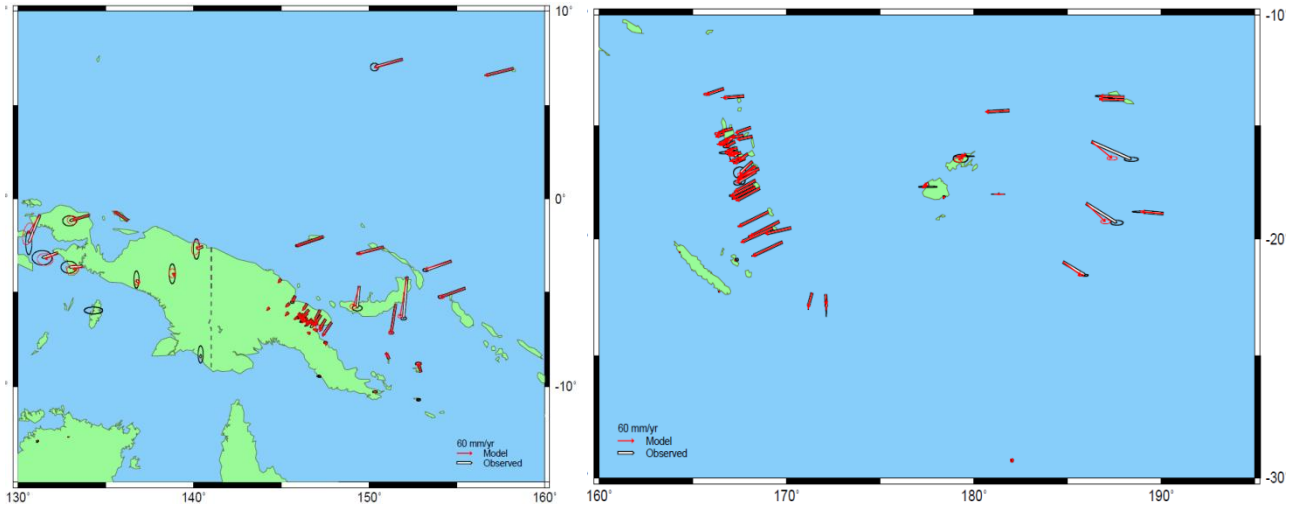

Figure 4. Modeled (red arrows) and observed (black and white arrows) horizontal GPS velocities relative to the fixed Australia plate for Papua New Guinea and Solomon Islands region (left panel), and Vanuatu, Fiji, and Tonga region (right panel).

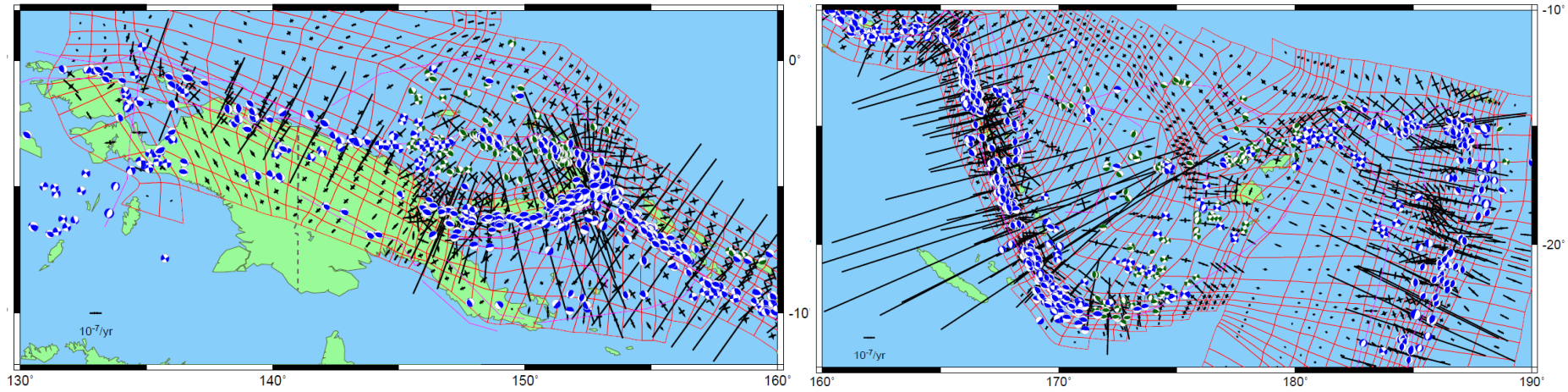

Figure 5. Predicted strain rate field (black arrows) for Papua New Guinea and Solomon Islands region (left panel), and for the Vanuatu, Fiji, and Tonga region (right panel). The beach-balls show the focal mechanisms of historical earthquakes: green refers to earthquakes with $5.3 \leq M_w \leq 6.0$, which are shown only for non-subduction areas; blue refers to earthquakes with $M_w > 6.0$. The red lines illustrate curvilinear grids and the thin pink lines illustrate the subduction zones and faults.

Based on regional tectonic, geologic, and seismic information, and the spatial distribution of GPS data, the region was divided into 3648 curvilinear grid cells, which cover both rigid and deforming zones (Figure 3). (The grid cells in Figure 5 below will show only the deforming zones, which are allowed to deform in the inversion procedure.)

Figure 4 shows the modeled and observed horizontal velocities in the region, relative to the fixed Australia plate. The modeled velocities match the observed GPS vectors at most of the sites, but significant differences exist at some stations in the Tonga region, in the New Britain Island of Papua New Guinea, and in West Papua, Indonesia. These discrepancies may be due to the incompatibility between these GPS data and others. Figure 5 illustrates the predicted strain rate field for a large part of the South Pacific region. We also plotted the moment tensors of large earthquakes in the global CMT catalog (http://www.globalcmt.org/) as a verification of the modeled strain rate field. The predicted strain rate field is consistent with the plate motions, regional seismic moment tensor solutions, and observed GPS velocities. For example, the large strain rate at the southern New Hebrides subduction zone segment is in line with the large converging rate observed by GPS data. We converted the predicted strain rate field to seismic moment rate budget for each source zone and used the budget for modeling regional seismicity.

4. MODELING THE REGIONAL SEISMICITY

Our regional seismicity model comprises 58 source zones, which were delineated based on the regional seismotectonics and historical seismicity (Figure 1). These source zones capture subduction zones, fore arc and back arc regions, transform zones, and background area. For the regions around Vanuatu, the source zones are based on Suckale and Grünthal (2009), while for the region around Fiji the zones are based on Jones (1998). We used the same methodology to model the regional seismicity as in Rong et al. (2010) except that here we employed the results from the geodetic modeling to constrain the upper bound seismic moment rate for each source zone. For those subduction segments with possible cascading ruptures, various cascading scenarios were considered using a stochastic modeling scheme (Mahdyiar and Rong, 2006). The rate of subduction mega earthquakes of M_w 8.5-9.0 was modeled by a moment conservation principle as in Rong et al. (2010).

The seismicity model can be partially verified by comparing the modeled seismicity rates vs. historical seismicity rates. This has been done for each of the seismic source zones. For example, Figure 6 shows the cumulative magnitude-frequency distributions from the model (green curve) and historical catalog (red dots) for some zones around Vanuatu. The long tails of the green curves derive from the moment rate based on the geodetic model that is considerably higher than the historical moment rate.

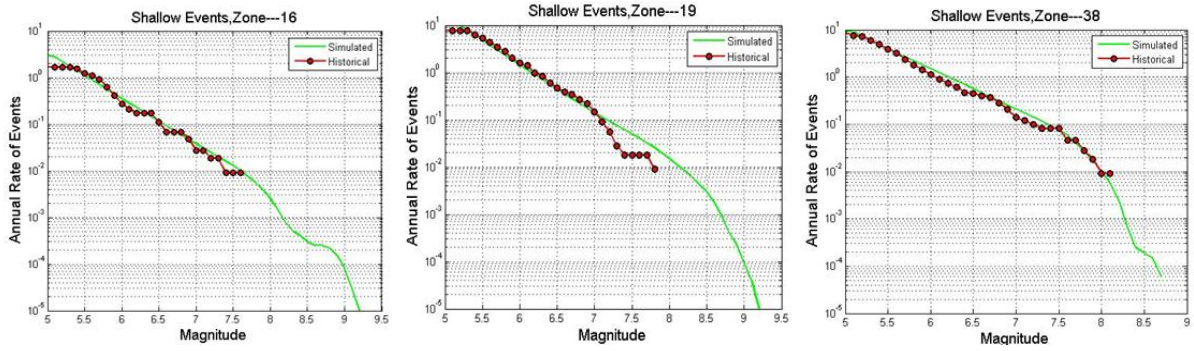

Figure 6. Cumulative magnitude-frequency distributions from the model (green curve) and from the historical catalog (red dots) for the source zones 16 (left), 19(middle), and 38 (right) around Vanuatu.

The modeled and historical seismicity rates are also compared at a larger scale. Figure 7 shows the excellent agreement between the magnitude-frequency distributions of modeled and historical earthquakes in areas around PNG and Fiji, respectively.

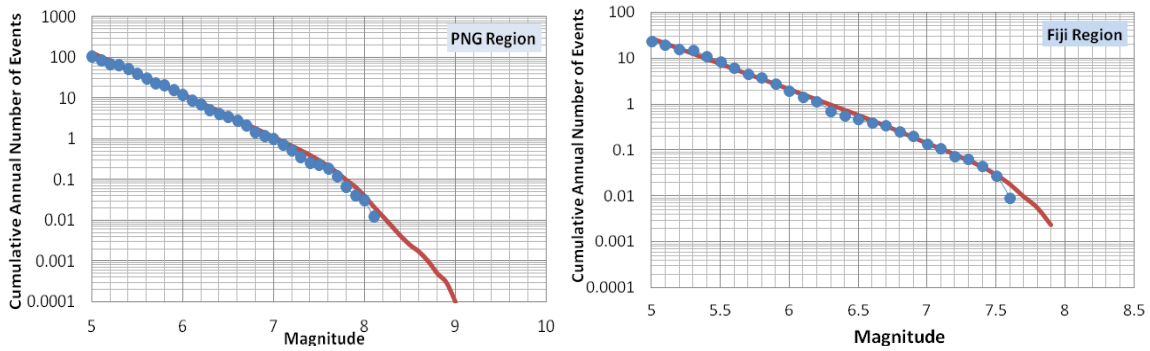

Figure 7. Cumulative magnitude-frequency distributions from the model (red curve) and historical catalog (blue dots) for large areas covering PNG (left), and Fiji (right).

5. PROBABILISTIC SEISMIC HAZARD MAPS

The hazard is computed using an earthquake catalog of simulated events consistent with the magnitude-frequency curves of the source zones. The synthetic catalog includes 10,000 realizations of next year seismicity and contains about 7.6 million events with $M_w \geq 5.0$. We applied a three-dimensional model to capture the spatial distribution of subduction interface, intraplate, and deep earthquakes. We used Benioff zone depth contours to define the subduction interface. Large subduction zone earthquakes are distributed along the subduction slab. Figure 8 illustrates the distribution of a sample 50-year simulated catalog. Both the spatial and the depth distributions are consistent with the historical earthquake catalog shown in Figure 2.

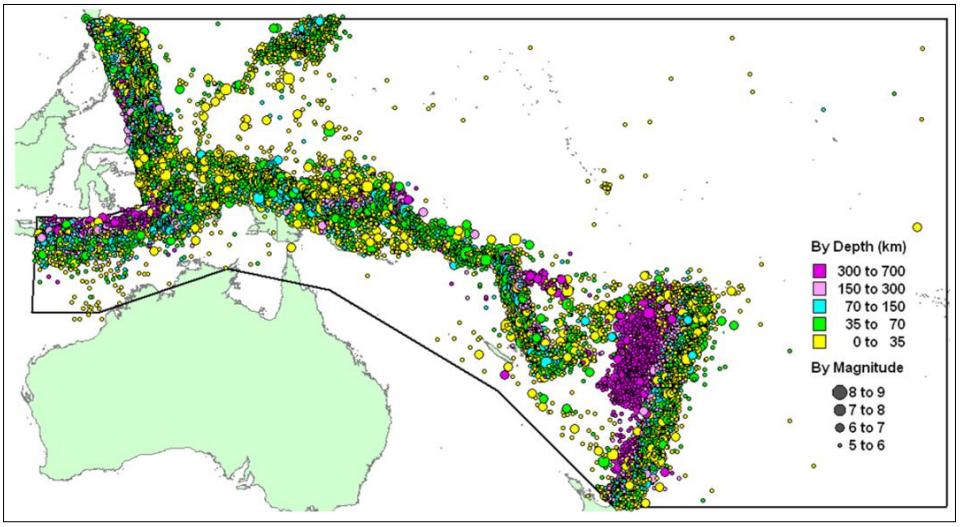

Figure 8. A sample 50-year synthetic catalog. Circles are color-coded by depth and sized by magnitude.

Seven ground motion prediction equations (GMPEs) were used to calculate ground motions. For crustal earthquakes, four Next Generation Attenuation (NGA) relation models of equal weight were used: Boore and Atkinson (2008), Campbell and Bozorgnia (2008), Chiou and Youngs (2008), and Abrahamson and Silva (2008). We adopted Youngs et al. (1997), Atkinson and Boore (2003), and Zhao et al. (2006) to estimate ground motion for subduction and deep earthquakes. Half the weight was given to Zhao et al. (2006), and the other half was split equally between Youngs et al. (1997) and Atkinson and Boore (2003). Due to the lack of GMPEs for oceanic earthquakes, the ground motion for this type of events was calculated using both crustal GMPEs and subduction GMPEs, with each type of GMPEs having half the weight. Given the size of the stochastic catalog, for each type of earthquake, we applied a single weighted average GMPE in the PSHA study. Strictly speaking, averaging GMPEs is probabilistically incorrect. However, this method provides in a manageable amount of time a close approximation to the average of the hazard results computed using each GMPE separately. In our

model, the geometry of all sources is formulated by a three-dimensional rupture area which assures that the distance calculation in the GMPEs is accurate and realistic.

Site conditions have a strong influence on earthquake ground motions and, therefore, on seismic hazard and risk estimates. Shorten et al. (2001) have derived seismic microzonation maps of four capital cities (Suva, Fiji; Port Vila, Vanuatu; Honiara, Solomon Islands; and Nuku'alofa, Tonga) by carrying out microtremor surveys. Given the lack of similar studies for all the other regions in the 15 countries, we derived site-condition maps based on high-resolution SRTM topography data (Jarvis et al., 2008) using the method of Allen and Wald (2009). Estimates of the shear wave velocity in the top 30 m of soil derived from the topography-based approach and the microzonation studies were embedded in the ground motion calculations. The probabilistic seismic hazard analysis (PSHA) included the ground motion intensity measures peak ground acceleration (PGA), and 5%-damped linear spectral accelerations at different oscillator periods. As an example of the results obtained, Figure 9 shows free surface PGA, including site effects, with 10% probability of exceedance in 50 years (i.e., 475-year mean return period) for some of the PICs.

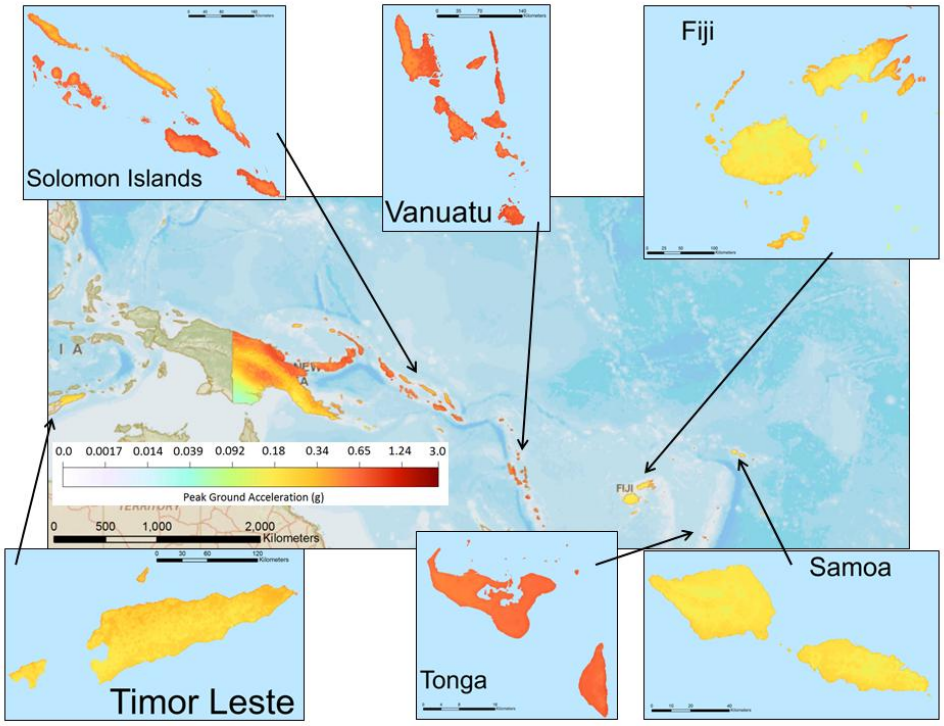

Figure 9. Map of free surface PGA, including site conditions, with 10% probability of exceedance in 50 years (475-year mean return period) for some of the Pacific Island Countries.

6. DISCUSSION

Figure 10 compares the hazard results from this study and the corresponding results from earlier studies. It shows that:

- In general, our estimates of the 475-year mean return period rock PGA values are closer to the results from the detailed local studies than to those from the GSHAP study.
- Historical seismicity in the neighborhood of the PICs does not explain the very similar 475-year rock PGA estimates for Kiribati, Marshall Islands, Micronesia, Nauru, Tuvalu, Samoa, Timor-Leste, and Tonga in the GSHAP study (Figure 10b) because: (1) Tonga is on the seismically active Tonga subduction zone, while Tuvalu, Kiribati, Marshall Islands, and Nauru are not only far from the regional subduction zones but are also located in seismically inactive areas; (2) Samoa is located at about 130 km north of the northern tip of the Tonga subduction zone; and (3) Timor-

Leste is in the middle of the seismically active Timor and Banda Sea trenches. The relative difference in the seismic hazard is correctly reflected in the PGA estimates from this study.

- It is important to account for site conditions in seismic hazard analysis. Based on the results from this study, the hazard with site conditions considered is about 20-30% higher than the rock hazard at the capitals of Vanuatu, Tonga, Timor-Leste and Micronesia, about 50% higher at the capital of Samoa, and more than 80% higher at the capitals of Tuvalu and Kiribati.

The seismic hazard maps presented here have sufficient details to be used in local seismic risk studies and were developed using the current state of practice in probabilistic seismic hazard assessment. The large differences between this study and GSHAP can be attributed to the combined impact of differences in earthquake source models, GMPEs, site conditions, and the details of the hazard calculations.

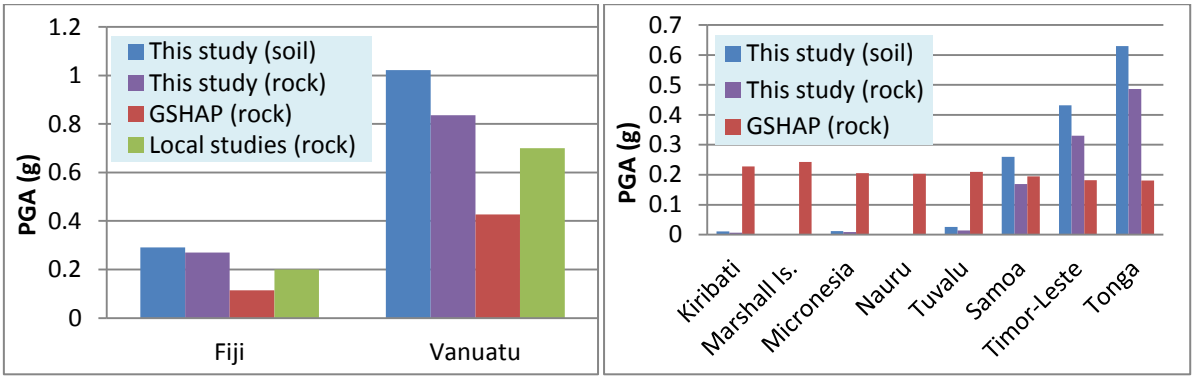

(a) (b)

Figure 10. Expected PGA (g), with a 10% probability of exceedance in 50 years (475-year mean return period), at the capitals of some of the PICs. The blue and purple bars are PGA values from this study with and without site conditions accounted for, respectively. The red bars are PGA values by GSHAP. The green bars in (a) are the results of local studies (Jones 1998 for Fiji; Suckale and Grünthal 2009 for Vanuatu).

AKCNOWLEDGEMENTS

The authors would like to thank Dr. Bingming Shen-Tu and Dr. Khosrow Shabestari of AIR Worldwide for constructive discussions. The financial support from World Bank and AIR Worldwide is appreciated.

REFERENCES

Abrahamson, N. and Silva, W. (2008). Summary of the Abrahamson & Silva NGA ground-motion relations. *Earthquake Spectra* **24**, 67-97.

Allen, T.I., Marano, K., Earle, P.S. and Wald, D.J. (2009). PAGER-CAT: A composite earthquake catalog for calibrating global fatality models. *Seism. Res. Lett.***80**, 57-62.

Allen, T.I. and Wald, D.J. (2009). On the use of high-resolution topographic data as a proxy for seismic site conditions (VS30). *Bull. Seism. Soc. Am.***99**, 935-943.

Atkinson, G.M. and Boore, D.M. (2003). Empirical ground motion relations for subduction-zone earthquakes and their application to Cascadia and other regions. *Bull. Seism. Soc. Am.***93**, 1703–1729.

Bevis, M., Taylor, F. W., Schutz, B. E., Recy, J., Isacks, B. L., Helu, S., Singh, R., Kendrick, E., Stowell, J., Taylor, B. and Calmantli, S. (1995). Geodetic observations of very rapid convergence and back-arc extension at the Tonga arc, *Nature* **374**, 249-251.

Bird, P. (2003). An updated digital model of plate boundaries, Geochemistry Geophysics Geosystems **4**, 1027, doi:10.1029/2001GC000252.

Boore, D.M., and Atkinson, G.M. (2008). Ground-motion prediction equations for the average horizontal component of PGA, PGV, and 5%-damped PSA at spectral periods between 0.01 s and 10.0 s. Earthquake Spectra 24, 99-138.

Bormann, P. and Saul, J. (2008). The new IASPEI standard broadband magnitude mB. *Seism. Res. Lett.* **79**, 698-706.

Calmant, S., Pelletier, B., Lebellegard, P., Bevis, M., Taylor, F. W. and Phillips, D. A. (2003). New insights on the tectonics along the New Hebrides subduction zone based on GPS results. *J. Geophys. Res.* **108**, 2319, doi:10.1029/2001JB000644.

Campbell, K.W. and Bozorgnia, Y. (2008). NGA ground motion model for the geometric mean horizontal component of PGA, PGV, PGD and 5% damped linear elastic response spectra for periods ranging from 0.01 to 10.0 s. *Earthquake Spectra* **24**, 139-171.

Chiou, B. and Youngs, R. (2008). An NGA model for the average horizontal component of peak ground motion and response spectra. *Earthquake Spectra* **24**, 173-215.

Engdahl, E.R., van der Hilst, R., and Buland, R. (1998). Global teleseismic earthquake relocation with improved travel times and procedures for depth determination. *Bull. Seism. Soc. Am.* **88**, 722–743.

Haines, A.J. and Holt, W.E. (1993). A procedure for obtaining the complete horizontal motions within zones of distributed deformation from the inversion of strain rate data. *J. Geophys. Res.* **98,** 12057-12082.

Haines, A.J., Jackson, J.A., Holt, W.E. and Agnew, D.C. (1998). Representing distributed deformation by continuous velocity fields. *Sci. Rept. 98/5*, Inst. of Geol. and Nucl.Sci., Wellington, New Zealand.

Jarvis, A., Reuter, H., Nelson, A. and Guevara, E. (2008). Hole-filled SRTM for the globe Version 4, available from the CGIAR-CSI SRTM 90m Database (http://srtm.csi.cgiar.org).

Jones T. (1998). Probabilistic earthquake hazard assessment for Fiji, Australian Geological Survey organization, AGSO Record 1997/46.

Kreemer, C., Holt, W.E. and Haines, A.J. (2003). An integrated global model of present-day plate motions and plate boundary deformation, *Geophys. J. Int.***154**, 8-34.

Mahdyiar, M. and Rong, Y. (2006). Stochastic simulation of multi-segment fault-cascading scenarios for earthquake hazard analysis. In the *proceedings of the 8th U.S. National Conference on Earthquake Engineering*, April 18-22, 2006, San Francisco, California, USA.

McCue, K. (1999). Seismic Hazard Mapping in Australia, the Southwest Pacific and Southeast Asia, *Annali Di Geofisica* **42**, 1191-1198.

Nishenko, S. P. (1991). Circum-Pacific seismic potential – 1989-1999. *Pure and Applied Geophysics* **135**, 169-259.

Puntodewo, S.S.O., McCaffrey, R., Calais, E., Bock, Y., Rais, J., Subarya, C., Poewariardi, R., Stevens, C., Genrich, J., Fauzi, Zwick, P. and Wdowinski, S. (1994). GPS measurements of crustal deformation within the Pacific-Australia plate boundary zone in Irian Jaya, Indonesia. *Tectonophysics* **237**, 141-153.

Rahiman, T.I.H. (2006). Neotectonics, seismic and Tsunami hazards, VitiLevu, Fiji. *Ph.D. thesis*, University of Canterbury.

Reasenberg, P. (1985). Second-order moment of central California seismicity, 1969-1982.*J. Geophys. Res.* **90**, 5479–5495.

Rong, Y., Mahdyiar, M., Shen-Tu, B., Shabestari, K.T. and Guin, J. (2010). Probabilistic seismic hazard assessment for South Pacific Islands. In the *proceeding of 9th US National Conference on Earthquake Engineering* (*9NCEE*), 25-29 July, 2010.

Shorten, G. and South Pacific Applied Geoscience Commission (2001). Site-specific earthquake hazard determinations in capital cities in the South Pacific. *SOPAC technical report* 300.

Simons, W.J.F., Socquet, A., Vigny, C., Ambrosius, B.A.C., Haji Abu, S., Chaiwat Promthong, Subarya C., Sarsiso, D.A., Matheussen, S., Morgan P. and Spakman, W.(2007). A decade of GPS in Southeast Asia: Resolving Sunda land motion and boundaries, J. *Geophys. Res.*, **112**, B06420, doi:10.1029/2005JB003868.

Suckale, J. and Grünthal, G. (2009). Probabilistic seismic hazard model for Vanuatu, *Bull. Seism.Soc. Am.* **99**, 2108-2126.

Tregoning, P., Lambeck, K., Stolz, A., Morgan, P., McClusky, S.C., van der Beek, P., McQueen, H., Jackson, R.J., Little, R.P., Laing, A., and Murphy, B., (1998). Estimation of current plate motions in Papua New Guinea from Global Positioning System observations. *J. Geophys. Res.* 103, 12,181–12,203.

Wallace, L. M., Stevens, C., Silver, E., McCaffrey, R., Loratung, W., Hasiata, S., Stanaway, R., Curley, R., Rosa, R. and Taugaloidi, J. (2004). GPS and seismological constraints on active tectonics and arc-continent collision in Papua New Guinea: Implications for mechanics of microplate rotations in a plate boundary zone. *J. Geophys. Res.* **109**, B05404, doi:10.1029/2003JB002481.

Youngs, R.R., Chiou, S.J., Silva, W.J. and Humphrey, J.R. (1997). Strong ground motion attenuation relationships for subduction zone earthquakes, *Seism. Res. Lett.* **68**, 58–73.

Zhao, J.X., Zhang, J., Asano, A., Ohno, Y., Oouchi, T., Takahashi, T., Ogawa, H., Irikura, K., Thio, H., Somerville, P., Fukushima, Y. and Fukushima Y. (2006). Attenuation relations of strong ground motion in Japan using site classification based on predominant period. *Bull. Seism. Soc. Am.* **96**, 898–913.